SO_2 removal in pulse energized electrostatic precipitator with heat exchanger for marine diesel

A. Zukeran[1], Y. Sakuma[1], K. Mayahara[1], T. Inui[2], Y. Ehara[3]

[1] *Department of Electrical and Electronic Engineering, Kanagawa Institute of Technology, 1030 Shimoogino, Atsugi, Kanagawa, 243-0292, Japan*

[2] *Factory & Facility System Division, Fuji Electric Co., Ltd., 1 Fujimachi, Hino, Tokyo, 191-8502, Japan*

[3] *Department of Electrical and Electronic Engineering, Tokyo City University, 1-28-1, Tamazutsumi, Setagaya, Tokyo, 158-8557, Japan*

Corresponding author: *zukeran-akinori@ele.kanagawa-it.ac.jp*

Keywords: Electrostatic Precipitator, PM Removal, SO_2 Removal, Marine Diesel

1. Introduction

Diesel particulate matters (DPM) and SO_x in the exhaust gases emitted from marine diesel engines cause serious problems in human health and coastal environments. In 2008, to overcome this problem, the International Marine Organization (IMO) adopted the MARPOL 73/78 Convention Revised Annex VI [1]. The regulation typically requires the use of low-sulfur fuel to reduce the sulphate portion of PM emissions and SO_x emissions. In line with this Annex, the global sulphur fuel limit was lowered to 3.5% in 2012 to reduce PM and SO_x emissions. This limit is planned to be further lowered to 0.5% in 2020 or 2025 [2]. Alternatively, it is also permitted to use an exhaust gas cleaning aftertreatment system or similar machinery that can reduce emissions to the levels that should be achieved by using a low-sulfur fuel.

Seawater scrubbers for reduction of SO_x and DPM, which includes Dry soot, sulphate and soluble organic fraction (SOF), have begun to be installed on ships [3]. However, there are still unsolved problems, such as the need for an extensive installation area on ships and a large amount of seawater. As a method for improving the performance of the wet scrubber, the use of seawater electrolysis has been under study and development. This method includes producing alkaline water by electrolysis and spraying it into exhaust gas to efficiently reduce SO_x [4-7]. It also has the effect of removing CO_2 [6] and NO_x [8] from the exhaust gas by the NaOH and chlorine gas resulting from the electrolysis.

As for the removal of diesel particulate matters (DPM) in ship exhaust gas, various techniques have been studied and developed, such as the application of a diesel particulate filter (DPF) used in automobiles [9-10] as well as the use of electrostatic scrubbers [11-12], electrostatic cyclones [13], barrier dischargers [14], and electrostatic precipitators (ESP) using the Hole effect or electrohydrodynamics (EHD) [15-16].

Nishida et al. reported that cooling the diesel exhaust gas of approximately 573 K to approximately 423 K caused an increase in the concentrations of the DPM and soluble organic fractions (SOF) due to the condensation of volatile substances. They also demonstrated that those components could be efficiently removed by a single-stage ESP [17].

In this study, the authors have proposed an ESP with heat exchanger for removal DPM and SO_2 [18]. The experimental system consists of a water-cooled 4-cycle diesel engine (cylinder volume, 400 cc; output, 5.5 kW), a heat exchanger and an ESP. In the experiment, Bunker A (ENEOS LSA fuel oil; sulphur content, 0.09%) was used as a test fuel oil. The exhaust gas at a temperature of approximately 160 ℃ was cooled to 20 ℃ using the gas heat exchanger. The ESP was supplied with negative DC, positive DC and positive pulse high voltages to generate corona discharges. SO_2 and DPM concentrations were measured by an SO_2 monitor and a low volume air sampler, respectively.

2. Experimental method

Fig. 1 shows a schematic of the experimental system. The system consists of a water-cooled 4-cycle diesel engine (DA-3100SS-IV, manufactured by Denyo Co., Ltd; cylinder volume, 400 cc; output, 5.5 kW), a heat exchanger and an ESP. In the experiment, Bunker A (ENEOS LSA fuel oil; sulphur content, 0.61%) was used as a test fuel oil. The heat exchanger can cool the exhaust gas from approximately 160°C to 100-20°C using a refrigerant (city water) of approximately 20°C with a controlled flow rate. The cooled gas passes through the ESP, which removes DPM.

Fig. 2 shows the structure of ESPs. Two types of ESPs were used for experiments. Type A was used to investigate DPM removal efficiency. Type A consisted of a precharger and a collection unit. The precharger has a parallel-plate electrode structure composed of high-voltage application electrodes (110×130 mm) and grounded plate electrodes (130×150 mm) alternately arranged with a gap of 10 mm. The high-voltage application electrodes have sawtooth edges on their upstream and downstream sides, while the grounded electrodes have no such edges. All electrodes are made of stainless steel with a thickness of 0.8 mm. The precharger is supplied with DC voltage of 0 to 9.5 kV to generate negative corona discharge. The gas flow rate is 6.2 NL/s.

Type B was used to investigate SO_2 removal efficiency. It has a wire-to-plate electrode structure alternately arranged with a gap of 10 mm. The high-voltage application wire electrode is made of tungsten with a diameter of 0.26 mm. The ESP is supplied with negative DC, positive DC or positive pulsed high voltages. Negative DC and positive DC high voltages were between 7.5 and 10.5 kV. Positive pulsed peak voltage was between 6.0 and 13.5 kVp. The gas flow rate was 0.4 NL/s.

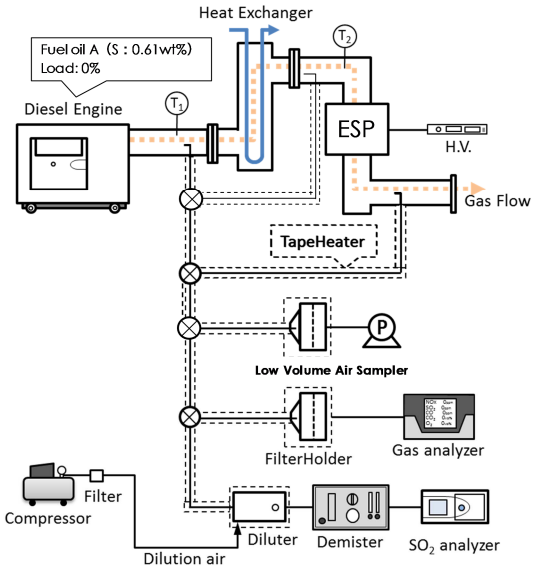

Figure 1. Schematic of the experimental system

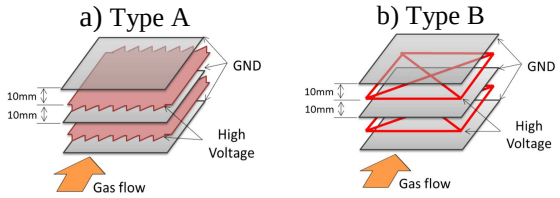

Figure 2. Structure of ESPs

To investigate the effect of our technique, we measured concentrations of DPM (SOF, SO_4^{2-} and Dry Soot) and SO_2 in the exhaust gas.

The DPM concentration in the exhaust gas was measured by drawing a portion of the exhaust gas using a low volume air sampler and passing it through a Teflon-coated glass-fiber filter to sample the DPM. The difference between the filter masses measured before and after the sampling was substituted in equation (1) to calculate the mass concentration C_{DPM} [mg/m^3]. The temperature of the sampling tube and filter holder was controlled by the tape heater so that it would be equal to the temperature of the drawn gas, in order to prevent the natural cooling of the sampling tube which may possibly cause condensation inside the tube and change the ratio of components.

$$C_{DPM} = \left(M_{DPM} - M_f\right) / \left(Q_L\ t_s\right) \qquad (1)$$

In equation (1), M_f and M_{DPM} are the filter masses [mg] before and after the DPM sampling, respectively. Q_L is the drawing rate [16.7×10^{-3} Nm^3/min] and t_s is the drawing time [5 min]. The filter mass was measured before and after the DPM sampling by drying the filter at 50°C for two hours in a thermostatic oven and subsequently weighing it.

From the filter thus sampled, the concentrations of the SOF, sulphate ion, bound H_2O and Dry Soot in the exhaust gas were analyzed. The analyzing procedure for each component was as follows:

After the DPM concentration (C_{DPM}) was measured, the SOF concentration C_{SOF} [mg/m^3] was calculated by subjecting the filter to a Soxhlet extraction with dichloromethane as the solvent and substituting into equation (2) the difference between the filter masses measured before and after the extraction. The filter was further subjected to ultrasonic washing to extract sulphate ion into ultrapure water. The extracted liquid was analyzed with an ion chromatograph to determine the sulphate ion concentration C_{SO4} [mg/m^3]. The bound-water concentration of the sulphuric acid C_{BW} [mg/m^3] was assumed to be 1.3 times the suphate ion concentration [19]. Finally, the Dry Soot concentration C_{DS} [mgm^3] was calculated by equation (3).

$$C_{SOF} = \left(M_{DPM} - M_{ext}\right) / \left(Q_L\ t\right) \qquad (2)$$

$$C_{DS} = C_{PM} - C_{SOF} - C_{SO4} - C_{BW} \qquad (3)$$

M_{ext} in equation (2) is the filter mass [mg] after the extraction of oil components.

To measure the SO_2 concentration, a portion of the exhaust gas was drawn from the duct and diluted by the diluter at the same temperature as the exhaust gas. The SO_2 concentration was measured with SO_2 analyzers based on a UV fluorescence method (APSA-370, HORIBA) or an infrared absorbing method (PG-350, HORIBA). The measured values were substituted into equations (4) to calculate the SO_2 removal rate η_{SO2}.

$$\eta_{SO2} = \left\{1 - \left(C_{SO2D} / C_{SO2U}\right)\right\} 100 \qquad (4)$$

In these equations, C_{SO2U} and C_{SO2D} are the SO_2 concentrations [mg/m^3] on the upstream and downstream sides of the apparatus, respectively.

3. Result and discussion

3.1. DPM removal rate

DPM removal rate was investigated using the type-A apparatus. Discharge current as a function of applied voltage for various gas temperatures is shown in Fig. 3. The corona onset voltage was 3.5 or 4.0 kV. Although the corona current increased with increasing applied voltage, the current at the same voltage decreased at lower gas temperatures.

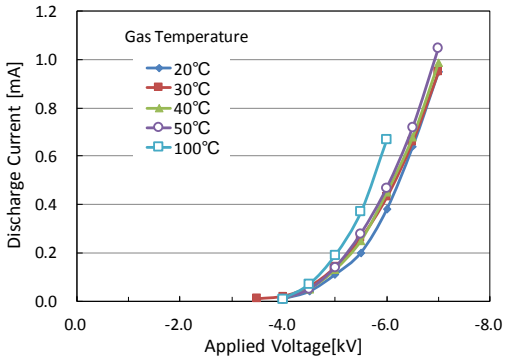

Figure 3. Discharge current as a function of applied voltage for various gas temperatures in type-A

The relationships between DPM mass concentration and the applied voltage are shown in Fig. 4.

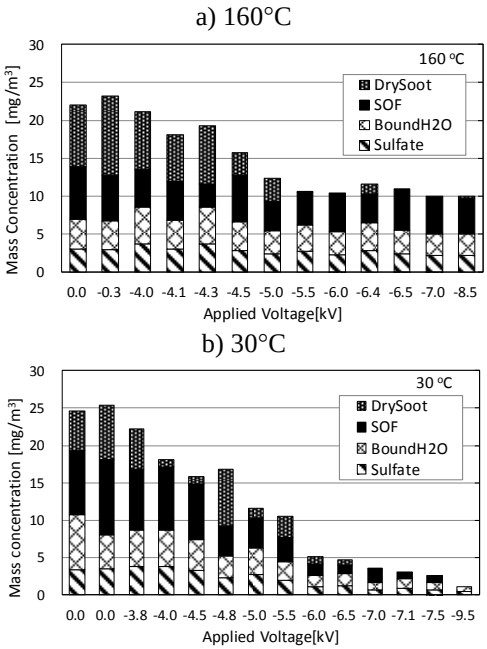

Figure 4. Relationships between DPM mass concentration and the applied voltage in type-A

The concentration at the downstream side of the ESP was measured. Fig. 4a and Fig. 4b are results obtained at the gas temperature of 160 and 30°C, respectively. The mass concentration of Dry Soot, SOF, bound H_2O and SO_4^{2-} are shown in Figures. In the result obtained at 160°C, DPM concentration, which is the total mass concentration, decreased at the voltages greater than approximately –4.0 kV, which was the corona onset voltage. The Dry Soot is almost removed at the voltage greater than –5.5 kV, whereas the other mass concentrations barely decreased. In the result obtained at 30°C as shown in Fig. 4b, the total mass concentration decreased with increasing voltage. Especially, all components significantly decreased compared with the result obtained at 160°C as shown in Fig. 4a. The relationships between DPM mass concentration and input power are shown in Fig. 5. Fig. 5a and Fig. 5b are results obtained at 160 and 30°C, respectively. For the same input energy, any component had a lower concentration at 30°C than at 160°C.

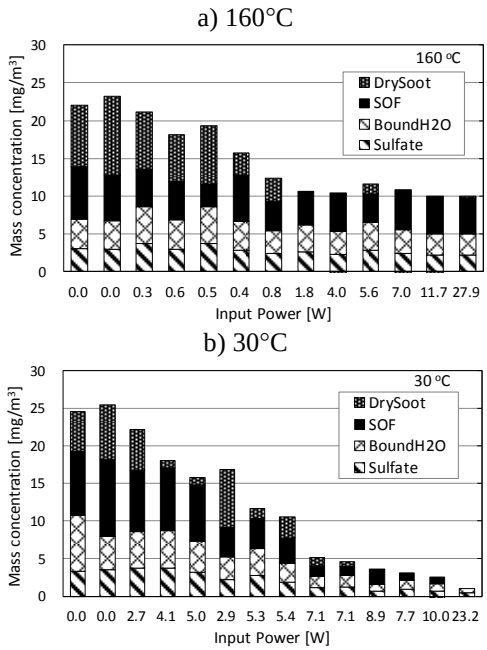

Figure 5. Relationships between DPM mass concentration and the input power in type-A

The relationship between SO_2 removal rate and the gas temperature is shown in Fig. 6. SO_2 concentration at the downstream side of the heat exchanger was measured without applying the voltage to the ESP. SO_2 removal rate increased with decreasing gas temperature, and that was stabilized at 28% within the range from 20 and 40°C, and condensed water was found. This is most likely because cooling the exhaust gas causes the condensation of water and the absorption of SO_2 in the gas into the condensed water.

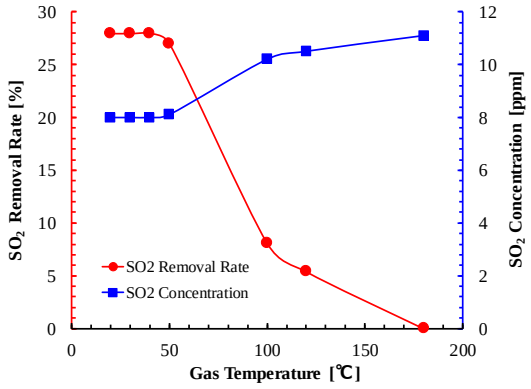

Figure 6. Relationship between SO_2 removal rate and gas temperature in type-A

This measurement was also performed with the voltage applied to the ESP, which suggested that the voltage has no influence on the SO_2 concentration under the condition of the type-A.

3.2. SO_2 removal rate

SO_2 removal rate was investigated using the type-B apparatus at the gas temperature of 60°C. The gas flow rate was lower than that of the type-A apparatus. The negative DC, the positive DC and the positive pulsed high voltages were applied to the ESP of the type-B.

The discharge current as a function of the applied voltage at the negative and the positive DC corona discharges is shown in Fig. 7.

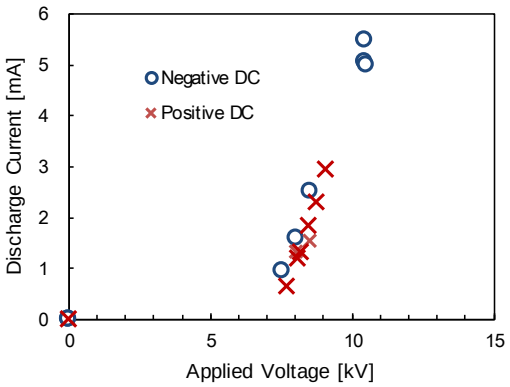

Figure 7. Discharge current as a function of the applied voltage at negative and positive DC corona discharge in type-B

Although both discharges showed similar characteristics, the spark voltage of the negative DC was greater than that of the positive DC. The corona discharge current was higher than that of type-A apparatus as shown in Fig. 3. The example wave forms of the pulsed voltage, current and power are shown in Fig. 8. The power W_t [W] at time t was calculated by equation (5).

$$W_t = V_t \times I_t \tag{5}$$

where V_t and I_t are the voltage [V] and current [A] at time t.

The peak voltage is 11 kV, and the rising time is approximately 70 ns as shown in Fig. 8a. The peak current is approximately 80 A, and the peak power is approximately 800 kW as shown in Fig. 8b and Fig. 8c. The pulsed high voltage can input large current and high power to the ESP in an instant.

SO_2 removal rate as a function of applied voltage for various cases is shown in Fig. 9. SO_2 removal rate increased at the voltages greater than 6 or 7 kV, which was the corona onset voltage. All cases roughly show similar characteristics.

SO_2 removal rate as a function of input power for various cases is shown in Fig 10. The input power W was calculated by equation (6).

$$W = f \int W_t dt \tag{6}$$

where f is frequency (250 Hz).

Although the peak power W_t is very high as shown in Fig. 8c, the input power is almost same as applied with the negative or the positive DC high voltages. SO_2 removal rate in every case increased with increasing input power, although the rate recorded in the case of the pulsed voltage is higher than in the other cases at the same input power.

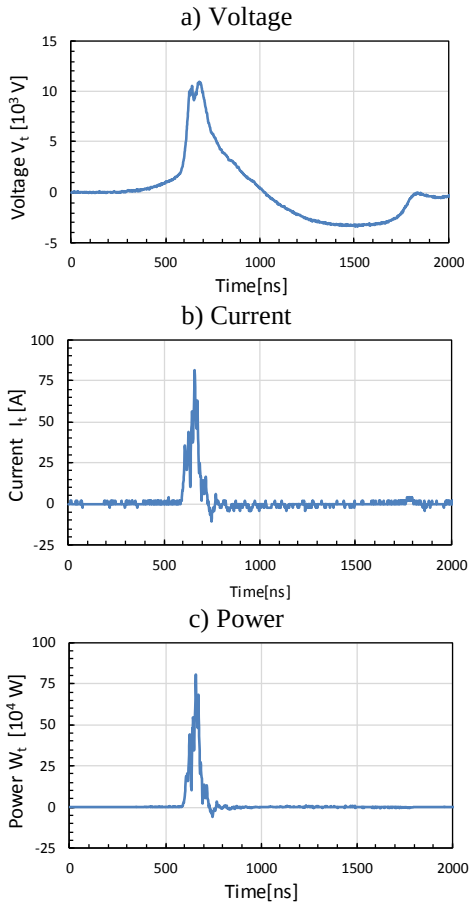

Figure 8. The example wave forms of the pulsed voltage, current and power

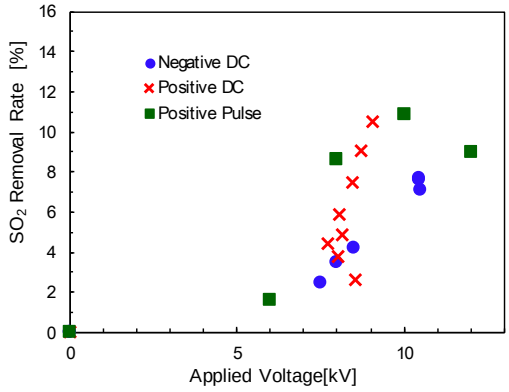

Figure 9. SO_2 removal rate as a function of applied voltage for various cases in type-B

The discharge luminescence observed in each case at the input power W of 20 W is shown in Fig. 11. The gas temperature was 20°C. Fig. 11a shows the appear-

ance of ESP with no voltage applied. Fig. 11b shows the luminescence of the negative DC corona discharge. Tuft corona discharge was observed on the surface of the wires. Fig. 11c is that of the positive DC corona discharge. Brush corona was observed along the wires. Streamer corona was also observed at a part of the area. Fig. 11d is the discharge luminescence observed when the positive pulsed voltage was applied to the ESP. The streamer corona expanded within the entire space.

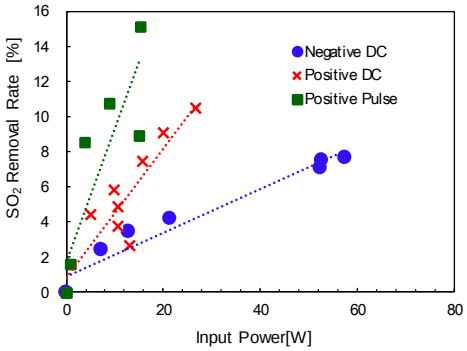

Figure 10. SO_2 removal rate as a function of input power for various cases in type-B

a) Appearance of ESP

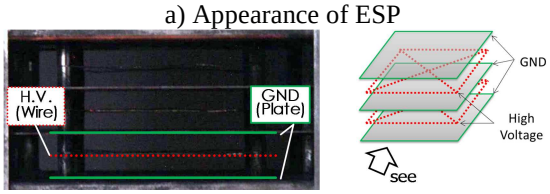

b) Negative DC corona discharge

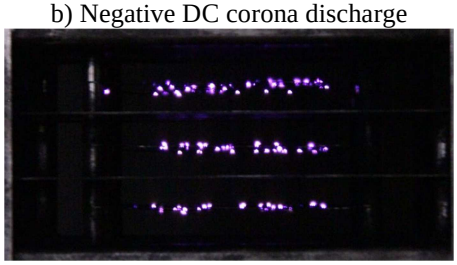

c) Postive corona discharge

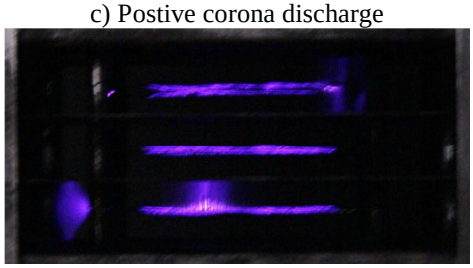

d) Positive puse corona discharge

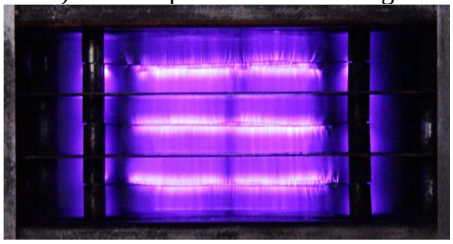

Figure 11. Discharge luminescence of each case at the input power of 20 W in type-B

These results indicate that the pulse energized ESP has the highest SO_2 removal rate in this study for the same input power, due to the instantaneously increasing discharge current and the streamer corona discharge.

The effect of cooling the exhaust gas on SO_2 removal rate in the pulse energized ESP is shown in Fig. 12. SO_2 removal rate at the gas temperature of 20°C and the applied voltage of 0 kV is 28% due to the effect of the cooling of the gas as shown in Fig. 6. SO_2 removal rate increased as the input power increased, and reached 40% at the input power of 20 W. The rate achieved with the cooling of the gas was constantly higher than that achieved without the cooling.

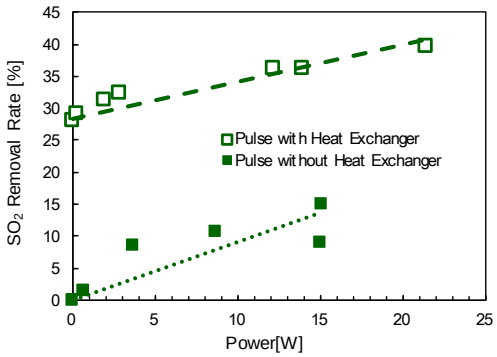

Figure 12. Effect of cooling the exhaust gas on SO_2 removal rate in the pulse energized ESP

4. Conclusion

In this study, experiments were carried out to improve the DPM and SO_2 removal rates in the ESP with the gas heat exchanger, and the following results were obtained:

(1) The Dry soot concentration included in DPM decreased with increasing voltage applied to the negative DC energized ESP without the heat exchanger, whereas the concentrations of SOF, bound H_2O and SO_4^{2-} barely decreased.

(2) The concentrations of Dry soot, SOF, bound H_2O and SO_4^{2-} decreased as the applied voltage increased in the negative DC energized ESP with the heat exchanger.

(3) The pulse energized ESP has a higher SO2 removal rate for the same input power than the negative and the positive DC energized ESPs.

(4) SO_2 removal rate in the pulse energized ESP with the heat exchanger is higher than that without the heat exchanger.

This work was supported by a Grant-in-Aid for Scientific Research (B), No. 15H04216, from the Japan Society for the Promotion of Science.

References

[1] International Maritime Organization (IMO); MARPOL 73/78 CONVENTION revised ANNEX VI, 2008.

[2] IMO; 2009 Guideline for exhaust gas clean-ing systems [resolution MEPC.184 (59)].

[3] Fuji Electric Co., Ltd., *Exhaust Gas Cleaning System for SOx and PM regulation compliance*, Catalog, 09Z1-E-0029, 2015.

[4] Nishida O., Sukheon A., Fujita H., Harano W. Tashiro M., Journal of the Japan Institution of Marine Engineering, 37, (9), 728-736, 2002.

[5] Inui T., Zukeran A., Asakawa D., Toyozumi H., Sawai J., Touyama H., Nakata E., Ehara Y., Journal of environmental conservation engineering, Vol. 44, No. 2, pp. 105-112, 2015.

[6] Inui T., Asakawa D., Toyozumi H., Zukeran A., Sawai J., Toyama H., Nakata E., Ehara Y., Journal of the JIME, Vol. 50, No. 1, pp. 113-118, 2015.

[7] Nishida O., Hosoda S., An S., Ihara A., Fujita H., Harano W., Hiroi M., Sato M., Aya T., Tashiro M., Journal of the Japan Institution of Marine Engineering, 38, (2), 81-86, 2003.

[8] Kawaji T., Nishida O., Fujita H., Harano W., Soo Kim H., Journal of The Japan Institution of Marine Engineering, 41, (3), 451-455, 2006.

[9] Maeda K., Tsuda M., Yamanishi D., Sudo N., Komori M., Journal of the Japan Institution of Marine Engineering, 48, (4), 93-98, 2013.

[10] Kuwabara T., Kuroki T., Yoshida K., Hanamoto K., Sato K., Okubo M., Journal of the Japan Institution of Marine Engineering, 48, (4), 117-122, 2013.

[11] Hong Ha T., Nishida O., Fujita H. Harano W., Journal of the Japan Institution of Marine Engineering, 44, (5), 2009.

[12] Takayama A., Fujita H. Harano W., Environmental Conservation Engineering, 42, (4), 228-234, 2013.

[13] Furugen M., Sasaki H., Takahashi T., Tsukamoto T., Journal of the Japan Institution of Marine Engineering, 48, (4), 87-92, 2013.

[14] Ehara Y., Journal of the Japan Institution of Marine Engineering, 48, (4), 105-110, 2013.

[15] Kawakami H., Zukeran A., Yasumoto K., Inui T., Enami Y., Ehara Y., Yamamoto T., International Journal of Plasma Environmental Science & Technolgy, 6, (2), 2012.

[16] Yamamoto T., a Mimura T., Otsuka N., Ito Y., Ehara Y., Zukeran A., IEEE Trans. Ind. Appl., 46, (4), 1606- 1611, 2010.

[17] I Made Ariana, Osami N., Hirotsugu F., Wataru H., Megumi F., Journal of the Japan Institution of Marine Engineering, 42, (2), 122-128, 2007

[18] Sakuma Y., Yamagami R., Zukeran A., Ehara Y., Inui T., *Journal of the JIME*, Vol49, No.4, pp.533-538, (http://www.jime.jp/e/publication /award_paper/pdf/2014AP5.pdf) 2014.

[19] Wall J.C., Hoekman S.K.; Fuel Composition Effects on Heavy-Duty Diesel Particulate Emissions, SAE Technical Paper Series, 841364, 1984.